Pseudospin partner bands in ^{130}Ba

S. Guo (郭松) ●,[1,2,*] C. M. Petrache,[3,†] D. Mengoni,[4] Y. X. Liu (刘艳鑫),[5] Q. B. Chen (陈启博),[6] Y. H. Qiang (强赟华),[1,2]
A. Astier,[3] E. Dupont,[3] K. K. Zheng (郑宽宽),[3] J. G. Wang (王建国),[1,2] B. Ding (丁兵),[1,2] B. F. Lv (吕冰锋),[1,2]
M. L. Liu (柳敏良),[1,2] Y. D. Fang (方永得),[1,2] X. H. Zhou (周小红),[1,2] D. Bazzacco,[4] A. Boso,[4] A. Goasduff,[4] F. Recchia,[4]
D. Testov,[4] F. Galtarossa,[7] G. Jaworski,[7] D. R. Napoli,[7] S. Riccetto,[7] M. Siciliano,[7] J. J. Valiente-Dobon,[7] C. Andreoiu,[8]
F. H. Garcia,[8] K. Ortner,[8] K. Whitmore,[8] B. Cederwall,[9] E. A. Lawrie,[10,11] I. Kuti,[12] D. Sohler,[12] T. Marchlewski,[13]
J. Srebrny,[13] and A. Tucholski[13]

[1]*Key Laboratory of High Precision Nuclear Spectroscopy, Institute of Modern Physics, Chinese Academy of Sciences,
Lanzhou 730000, People's Republic of China*
[2]*School of Nuclear Science and Technology, University of Chinese Academy of Science, Beijing 100049, People's Republic of China*
[3]*Université Paris-Saclay, CNRS/IN2P3, IJCLab, 91405 Orsay, France*
[4]*Dipartimento di Fisica e Astronomia dell'Università, and INFN, Sezione di Padova, 35131 Padova, Italy*
[5]*Department of Physics, Huzhou University, Huzhou 313000, People's Republic of China*
[6]*Physik-Department, Technische Universität München, D-85747 Garching, Germany*
[7]*INFN Laboratori Nazionali di Legnaro, 35020 Legnaro (Pd), Italy*
[8]*Department of Chemistry, Simon Fraser University, Burnaby, British Columbia V5A 1S6, Canada*
[9]*KTH Department of Physics, S-10691 Stockholm, Sweden*
[10]*iThemba LABS, National Research Foundation, P.O. Box 722, 7131 Somerset West, South Africa*
[11]*Department of Physics, University of the Western Cape, Private Bag X17, 7535 Bellville, South Africa*
[12]*Institute for Nuclear Research, Hungarian Academy of Sciences, H-4026 Debrecen, Hungary*
[13]*Heavy Ion Laboratory, University of Warsaw, 02-093 Warsaw, Poland*

The high-spin states in ^{130}Ba have been investigated using the ^{122}Sn(^{13}C, $5n$) reaction and the GALILEO array coupled to the EUCLIDES and Neutron Wall ancillary detectors. The level scheme has been extended to an excitation energy of $\approx$12 MeV and spin 28. Two sets of pseudospin partner bands have been identified built on $\pi h_{11/2}(g_{7/2}, d_{5/2})$ and $\nu h_{11/2}(s_{1/2}, d_{3/2})$ configurations. The assignments are supported by calculations using the projected shell model and the particle rotor model.

I. INTRODUCTION

Recently, a set of pseudospin-chiral quartet bands built on the $\pi h_{11/2}(g_{7/2}, d_{5/2}) \otimes \nu h_{11/2}$ configuration was reported in ^{131}Ba [1]. It is the first experimental observation of the coexistence and coupling of chiral and pseudospin symmetries. As a fundamental symmetry, chiral symmetry spontaneous breaking should occur in triaxial deformed nuclei [2]. The pseudospin has also been interpreted as a relativistic symmetry of the Dirac Hamiltonian [3]. The structure of quartet bands shows that the energy degeneracy caused by the pseudospin symmetry is comparable to that caused by chirality. In the $A \approx 130$ mass region, more than 30 chiral doublet bands have been reported [4]. On the other hand, only a few pseudospin partner bands have been observed experimentally [5–10], leading to ambiguous understanding of their mechanism and the difficulty of distinguishing them from other doublet bands. An empirical rule has been suggested that

opposite phases can be found in the $B(M1)/B(E2)$ staggering for pseudospin partner bands, while the same phases are expected for chiral doublet bands [5,11]. However, the application of this rule is limited, since no clear staggering can be deduced for some doublet bands [6]. Moreover, pseudospin partner bands were misinterpreted as signature pairs in some early works [7,12]. More efforts are required to distinguish different types of doublet bands, especially for pseudospin partner bands.

In ^{129}Cs, pseudospin partner bands have been identified, built on the $\pi(g_{7/2}, d_{5/2})$ configuration [7,12]. Therefore, a pair of corresponding two-quasiparticle pseudospin partner bands is expected to exist in ^{130}Ba, which lies in between ^{129}Cs and ^{131}Ba. The quasineutron in ^{130}Ba can also occupy other pseudospin partner orbitals $\nu(s_{1/2}, d_{3/2})$, providing a chance to search for pseudospin partner bands built on neutron configuration.

The spectroscopic study of the ^{130}Ba nucleus has a long history: the $K^{\pi} = 8^-$ isomer identified in 1966 by Brinckmann [13] was studied subsequently in Refs. [14–17], the low-spin states were studied in Refs. [18–22], and the high-spin states in Refs. [23–29].

---

*Corresponding author: gs@impcas.ac.cn
†Corresponding author: petrache@csnsm.in2p3.fr

Numerous theoretical studies were devoted to the Ba nuclei with $N < 82$, and an exhaustive list of references is not easy to establish. However, the theoretical papers published until 2015 can be found in the introductions of Refs. [30,31]. No article focused on the high-spin structure of the barium nuclei has been published since 2001. The calculated energy spectra and deformations of the high-spin states are based on microscopic or microscopic-macroscopic models employing the Harteee-Fock-Bogoliubov mean field [32], the Woods-Saxon potential [33–35], or the PC-PK1 interaction [17]. Algebraic models like the interactig boson model (IBM) [36] for the low-lying states, which reflect the varying features ranging from U(5) towards SU(3) via O(6) for nuclei with $N = 66$ to $N = 78$, have also been published [31], triggered by interest in the E(5) critical point symmetry [37,38].

The present paper reports new experimental results both at low and at high spins in ^{130}Ba, which were obtained from a high statistics experiment performed using the GALILEO spectrometer and the ^{122}Cd(^{13}C, $5n$) reaction. The observed bands are discussed in the context of the particle rotor model (PRM) described in Ref. [39].

Partial results of this experiment, particularly the band above the $K^\pi = 8^-$ long-lived isomer, were reported in a previous article [17], completing the systematics of bands built on top of the 8^- isomers in the $N = 74$ isotones and confirming the $\nu[514]9/2^-[404]7/2^+$ two-neutron configuration. In another previous paper [29], we reported rotational bands based on different shapes and different orientations of rotation. Specifically, the t band is first observed in the $A = 130$ mass region. From a straightforward view, band S1′ was regarded as the unfavored signature branch of band S1. However, it was also mentioned that the calculated signature splitting was apparently larger than the experimental one, which implies an alternative explanation other than the signature partner branch. Later it was suggested to be the first wobbling candidate built on a two-quasiparticle configuration [40].

The details of the experimental setup are presented in Sec. II. The results of the data analysis are presented in Sec. III. The configurations of the different bands are discussed in Sec. IV. The summary is given in Sec. V.

II. EXPERIMENTAL DETAILS

The ^{130}Ba nucleus was populated via the ^{122}Sn(^{13}C, $5n$) reaction at a beam energy of 65 MeV. The ^{13}C beam of 5 p nA was provided by the XTU Tandem accelerator of the Laboratori Nazionali di Legnaro. The target consisted of a stack of two self-supporting ^{122}Sn foils with a thickness of 0.5 mg/cm^2 each. The ^{130}Ba nucleus is among the most intensely populated nuclei via the $5n$ reaction channel, with about 40% of the fusion-evaporation cross section, as calculated with the PACE4 code [41]. The γ rays were detected by the GALILEO spectrometer, which consisted of 25 Compton-suppressed high-purity germanium (HPGe) detectors placed on four rings at 90° (10 detectors), 119° (5 detectors), 129° (5 detectors), and 152° (5 detectors). To distinguish different reaction channels, charged particles and neutrons were

detected by the EUCLIDES silicon ball [42] and the Neutron Wall array [43,44], respectively.

Data were recorded by the GALILEO data acquisition system which was designed for the GALILEO-EUCLIDES Neutron Wall Experiment [45]. The accumulated data were unfolded and sorted into files in the ROOT format, while Doppler shifts in energy were corrected using a recoil velocity $\beta = v/c = 0.0095$, determined from comparing peak energies acquired by detectors at different rings. A total of 1.2×10^9 triple- or higher-fold events have been collected. The coincidence events were sorted into a three-dimensional histogram (cube) and the analysis was carried out with the RAD-WARE software package [46,47]. A series of two-dimensional histograms (matrices) were also built in coincidence with different sets of detected particles (e.g., p, α, n, $2n$, pn, αn, etc.), which helped us to assign new transitions to different nuclei and to eliminate or identify contaminants.

A two-point angular-correlation ratio, R_{ac} [48], using the detectors placed at 90° and 152°, was employed to deduce the transition multipolarities. The mixing ratios (δ) of the $M1/E2$ transitions were deduced from the transition intensities measured at the four angles available in the GALILEO array (see above), and employing a method developed by Matta [49,50] for the analysis of angular-distribution measurements. For many transitions there are two solutions for δ in the χ^2 plot, with the absolute values larger and smaller than 1. It is unlikely that there are predominantly $E2$ ($\Delta I = 1$) transitions in dipole bands, which normally have predominantly $M1$ transitions. For all transitions analyzed in the present work, the δ values smaller than 1 have been adopted. Still, we cannot completely exclude the larger values only by angular correlation/distribution measurements.

III. RESULTS AND LEVEL SCHEME

The partial level schemes showing separately the positive-parity and negative-parity states of ^{130}Ba are shown in Fig. 1. The present level schemes are mainly developed on the basis of those reported in Refs. [23,25,28] with a few modifications, while the 3^- state in N1 was first reported in Ref. [21]. Newly observed structures are marked in red. Comparing to previous works, the level schemes are considerably extended and several new dipole and quadrupole sequences have been identified. Most of the identified transitions were grouped into bands: the ground state band (GSB), the γ band, S bands (S1, S1′, S2p, S2o, S2o′, S2″), tilted rotation band (t band), six negative-parity bands (N1–N6) and two dipole bands (D1, D2). Most of transitions out of these bands are grouped into fragmented structures (F1–F6). Typical double coincidence spectra are shown in Fig. 2. In the present work, thin targets with no backing were used, and the produced nuclei leave the center of the detector array in a few nanoseconds. Therefore the decay from the 8^- K isomer ($T_{1/2} = 9.4$ ms) is not observed in this work. Transition energies and intensities, angular distribution coefficients and anisotropies, as well as suggested spins and parities are given in Table I. In the present article, several figures show the excitation energies and other values deduced from them. Since the typical error for most transition energies is smaller than 0.5 keV, the error bars of
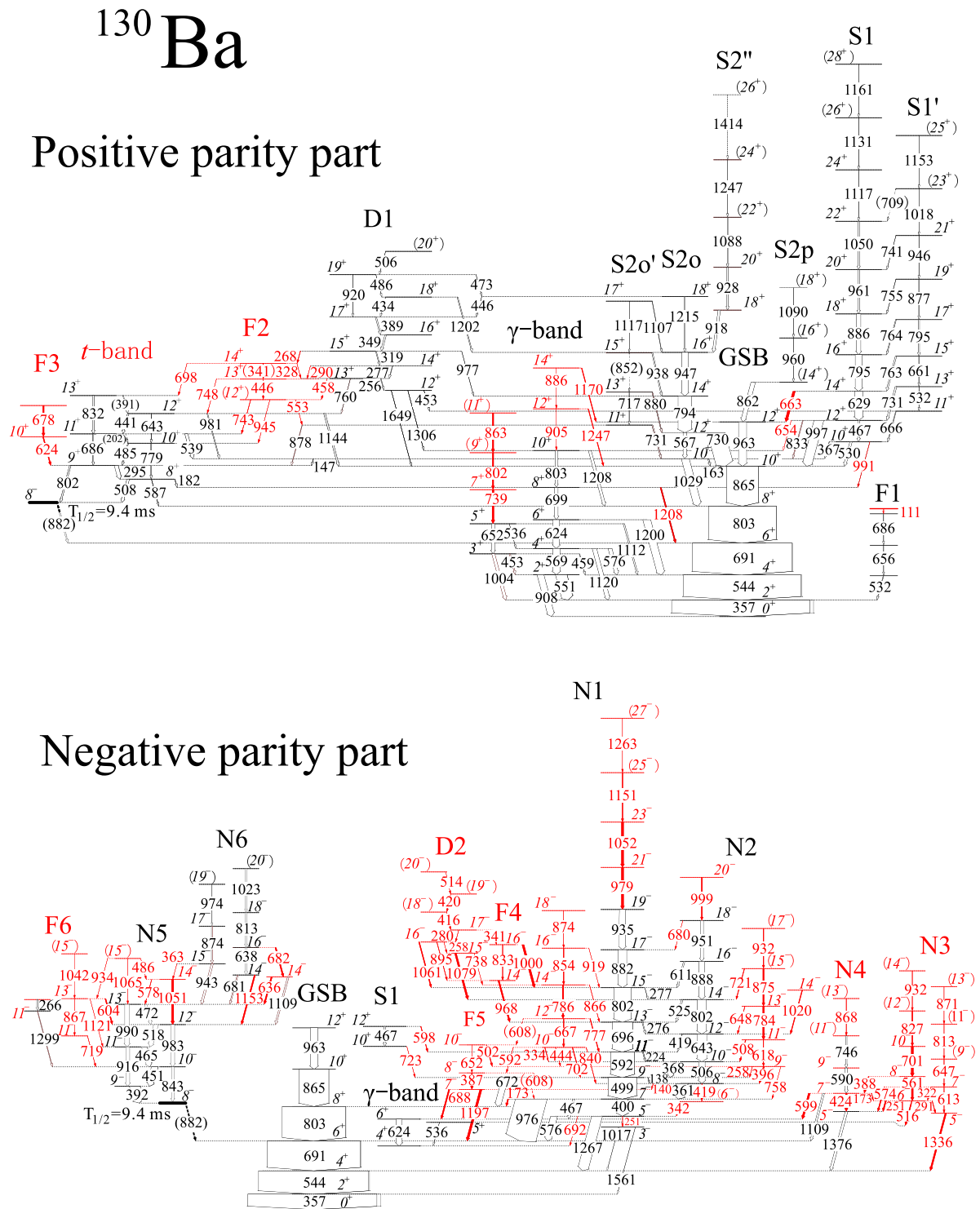
FIG. 1. Level scheme of ^{130}Ba. Newly observed structures reported in the present work and in our previous articles [17,29] are marked in red. The energies of the transitions are given in keV, and the widths of the arrows are relative to γ intensities.

experimental points are much smaller than the symbol size in these figures, and they are not plotted.

The modifications on the previously reported level schemes are interpreted below.

Prior to the present work, the γ band was reported up to the 7^+ and 10^+ states for odd and even spin states, respectively. A state at 2474 keV, feeding the 5^+ state by a 462-keV

transition, was first identified in Ref. [23], and assigned to the 7^+ state in Ref. [28]. However, the 462-keV transition was reassigned to deexcite the 8^-, 2475-keV isomer in Ref. [16]. The latter assignment is supported by the present work, since this transition is not observed in the thin-target measurement.

The cascade F1 was reported previously in Ref. [23], and confirmed in Ref. [28]. In the present work, a new
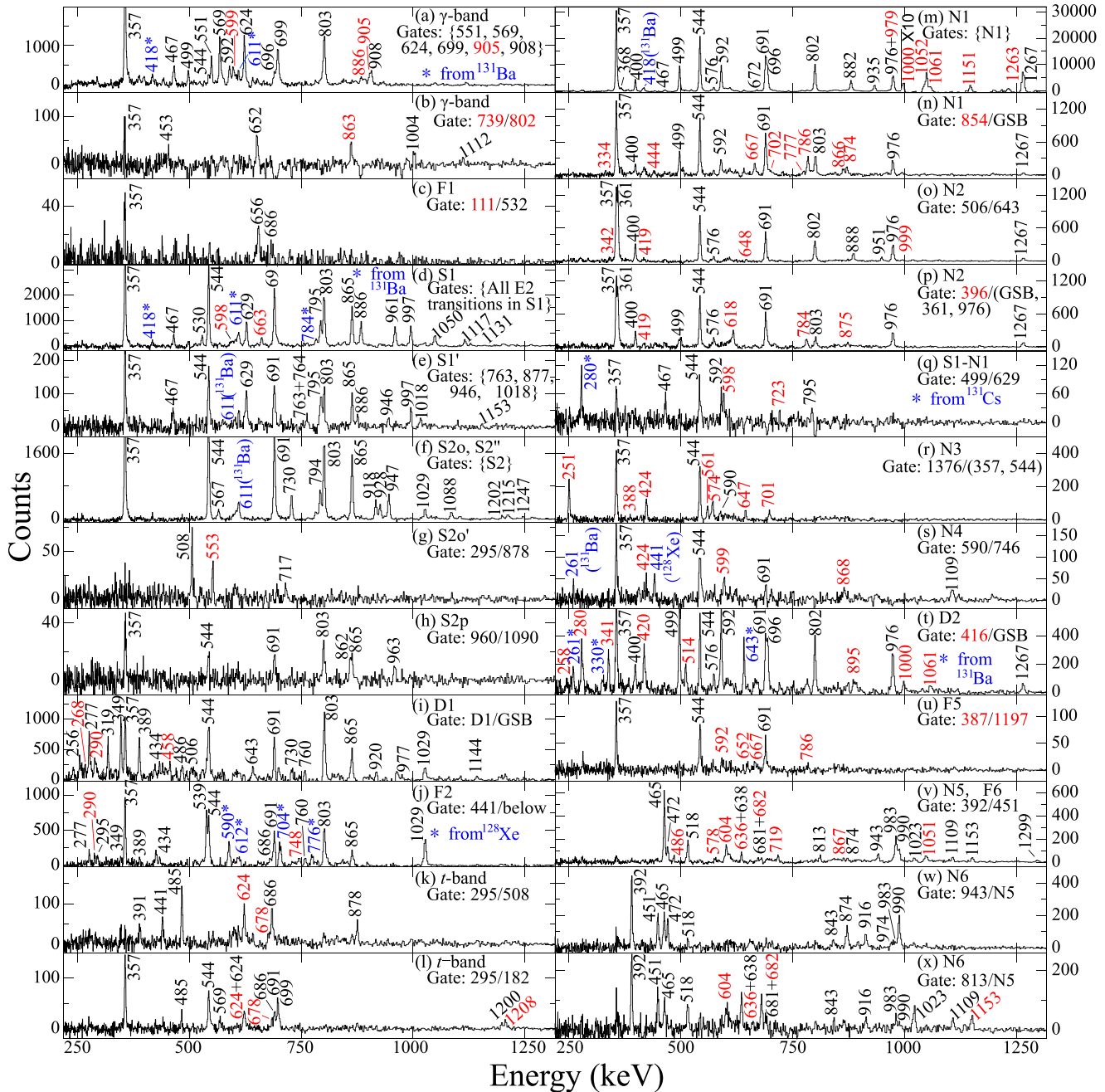
FIG. 2. Typical double-gated coincidence spectra for the new structures in ^{130}Ba. The structure to be supported and the gating information are marked in the up right corner of each spectrum. For figures (a), (d), (e), (f), and (m), the spectra are obtained by summing the spectra double-gated on all combinations of the transitions in the curly braces. For figures (i), (j), (n), (p), (r), (t), (w), and (x), the spectra are obtained by summing the spectra with a gate on the transitions before the slash, and a second gate on the transitions after the slash. In the gating information of figures (i), (n), (p), and (t), GSB stands for the transitions of 357, 544, and 691 keV in the GSB. Similarly, S2 stands for the transitions of 567, 730, 794, 947, 918, 928, and 1088 keV in bands S2o and S2″ for figure (f), D1 stands for the $\Delta I = 1$ transitions between states from 12^+ and 18^+ in band D1 for figure (i), N1 stands for the $\Delta I = 2$ transitions between states from 7^- and 25^- in band N1 for figure (m), and N5 stands for all in-band transitions below 12^- in N5 for figures (w) and (x). For figure (j), "below" means transitions of 357, 539, 544, 691, 803, and 1029 keV below the 441-keV transition. Newly observed transitions are marked in red, and contaminants from other nuclei are labeled in blue.

111-keV transition is found to be in coincidence with the known sequence, and is tentatively placed above it. This sequence is rather weak in the present measurement, with intensities of approximately one order of magnitude less than those reported in Ref. [25]. Considering that backings were used in the previous work to stop the residues, the loss of intensity may originate in an isomer with a lifetime of several hundred nanoseconds.

TABLE I. Energies of initial states, transition energies, relative γ-ray intensities normalized to the intensity of the 357-keV transition in the ground state band which is set to 1000, spin and parity assignments, bands the final states belong to, angular correlation ratios (R_{ac}), and $E2/M1$ mixing ratios (δ) for $M1/E2$ transitions in ^{130}Ba. Transitions are grouped in bands by their initial states. For transition energies E_γ, one significant digit after the decimal point is reserved when the error is smaller than 0.5 keV. Otherwise the transition energies are shown as integers. The γ-ray intensities T_γ are not given for those transitions which are too weak and/or contaminated. Generally their intensities are smaller than 2. Spin-parity assignments that are tentative are given in parentheses.

E_i (level)	E_γ (keV)	T_γ	$I_i^\pi \to I_f^\pi$	Final state band	R_{ac} ratio	Mult.	δ
GSB							
357.4	357.4	1000(22)	$2^+ \to 0^+$	GSB	1.48(5)	$E2$	
901.8	544.4	853(23)	$4^+ \to 2^+$	GSB	1.34(7)	$E2$	
1593.2	691.4	720(25)	$6^+ \to 4^+$	GSB	1.46(3)	$E2$	
2396.0	802.8	492(50)	$8^+ \to 6^+$	GSB	1.38(4)	$E2$	
3261.2	865.2	229(7)	$10^+ \to 8^+$	GSB	1.40(4)	$E2$	
4224.5	963.3	58(3)	$12^+ \to 10^+$	GSB	1.75(37)	$E2$	
γ band							
908.0	908.0	48(3)	$2^+ \to 0^+$	GSB	1.39(10)	$E2$	
	550.6	81(5)	$2^+ \to 2^+$	GSB	0.97(3)	$M1/E2$	
1361.1	453.2	8(2)	$3^+ \to 2^+$	γ band		$M1/E2$	
	1003.9	22(2)	$3^+ \to 2^+$	GSB	1.01(3)	$M1/E2$	
	459.3	3(1)	$3^+ \to 4^+$	GSB		$M1/E2$	
1477.4	569.3	52(4)	$4^+ \to 2^+$	γ band	1.23(5)	$E2$	
	1119.8	31(2)	$4^+ \to 2^+$	GSB	1.31(6)	$E2$	
	575.5	27(2)	$4^+ \to 4^+$	GSB	0.96(3)	$M1/E2$	
2012.8	651.7	23(2)	$5^+ \to 3^+$	γ band	1.27(8)	$E2$	
	535.8		$5^+ \to 4^+$	γ band		$M1/E2$	
2101.7	624.1	46(8)	$6^+ \to 4^+$	γ band	1.42(5)	$E2$	
	1199.8	55(2)	$6^+ \to 4^+$	GSB	1.39(9)	$E2$	
2751.4	738.6	14(1)	$7^+ \to 5^+$	γ band		$E2$	
2801.1	699.4	25(7)	$8^+ \to 6^+$	γ band	1.45(6)	$E2$	
	1208.1	9(3)	$8^+ \to 6^+$	GSB	1.51(20)	$E2$	
3553.7	802.3	10(2)	$(9^+) \to 7^+$	γ band			
3603.6	802.5	16(5)	$10^+ \to 8^+$	γ band	1.38(4)	$E2$	
	1208.4	20(7)	$10^+ \to 8^+$	GSB	1.27(9)	$E2$	
4417	863		$(11^+) \to (9^+)$	γ band			
4508.6	905		$12^+ \to 10^+$	γ band	1.34(11)	$E2$	
	1247.4	5(1)	$12^+ \to 10^+$	GSB	1.52(20)	$E2$	
5394.8	886		$14^+ \to 12^+$	γ band	1.46(52)	$E2$	
	1170.3	5(1)	$14^+ \to 12^+$	GSB	1.81(19)	$E2$	
S1							
3791.4	530.2	16(2)	$10^+ \to 10^+$	GSB	1.37(10)	$M1/E2$	
	366.5	2(1)	$10^+ \to 10^+$	S2o		$M1/E2$	
	990.8	2(1)	$10^+ \to 8^+$	γ band		$E2$	
	723.4	2(1)	$10^+ \to 9^-$	N1		$E1$	
4257.9	466.6	14(3)	$12^+ \to 10^+$	S1	1.29(4)	$E2$	
	996.7	68(8)	$12^+ \to 10^+$	GSB	1.35(5)	$E2$	
	833.4	5(1)	$12^+ \to 10^+$	S2o	1.84(27)	$E2$	
	654.2	$\leqslant 2$	$12^+ \to 10^+$	γ band	1.67(16)	$E2$	
	597.8	4(1)	$12^+ \to 11^-$	N1		$E1$	
4887.2	629.3	59(3)	$14^+ \to 12^+$	S1	1.40(18)	$E2$	
	663.3	18(4)	$14^+ \to 12^+$	GSB	1.60(8)	$E2$	
5682.1	794.9	51(7)	$16^+ \to 14^+$	S1	1.48(6)	$E2$	
6567.6	885.5	31(3)	$18^+ \to 16^+$	S1	1.45(9)	$E2$	
7528.4	960.8	13(2)	$20^+ \to 18^+$	S1	1.49(7)	$E2$	
8578.5	1050.1	11(1)	$22^+ \to 20^+$	S1	1.33(9)	$E2$	
9695.2	1116.7	3(1)	$24^+ \to 22^+$	S1	1.52(24)	$E2$	
10825.8	1130.6	2(1)	$(26^+) \to 24^+$	S1			
11986.6	1160.8		$(28^+) \to (26^+)$	S1			

TABLE I. (*Continued.*)

E_i (level)	E_γ (keV)	T_γ	$I_i^\pi \to I_f^\pi$	Final state band	R_{ac} ratio	Mult.	δ
S1′							
4457.6	665.9	4(1)	$11^+ \to 10^+$	S1	0.71(7)	$M1/E2$	−0.06(7)
4989.3	731.4	12(1)	$13^+ \to 12^+$	S1	0.23(3)	$M1/E2$	−0.58(13)
	531.7	2(1)	$13^+ \to 11^+$	S1′		$E2$	
5650.0	762.6	10(2)	$15^+ \to 14^+$	S1	0.19(2)	$M1/E2$	−0.62(10)
	661.4	4(1)	$15^+ \to 13^+$	S1′	1.56(19)	$E2$	
6444.8	764.2	6(1)	$17^+ \to 16^+$	S1	0.19(2)	$M1/E2$	−0.62(10)
	794.7	9(2)	$17^+ \to 15^+$	S1′		$E2$	
7322.0	755.3	2(1)	$19^+ \to 18^+$	S1		$M1/E2$	
	876.7	4(1)	$19^+ \to 17^+$	S1′	2.00(42)	$E2$	
8269.1	740.9		$21^+ \to 20^+$	S1		$M1/E2$	
	946.1	2(1)	$21^+ \to 19^+$	S1′	1.33(19)	$E2$	
9286.7	(709)		$(23^+) \to 22^+$	S1			
	1017.6		$(23^+) \to 21^+$	S1′			
10440	1153		$(25^+) \to (23^+)$	S1′			
S2o							
3424.6	1028.6	55(2)	$10^+ \to 8^+$	GSB	1.62(7)	$E2$	
	163.4	7(2)	$10^+ \to 10^+$	GSB	1.79(14)	$M1/E2$	
	146.8		$10^+ \to 9^+$	t band		$M1/E2$	
3991.2	566.7	26(3)	$12^+ \to 10^+$	S2o	1.64(8)	$E2$	
	730.0	124(35)	$12^+ \to 10^+$	GSB	1.67(10)	$E2$	
4785.2	794.0	98(16)	$14^+ \to 12^+$	S2o	1.47(4)	$E2$	
5732.5	947.3	47(3)	$16^+ \to 14^+$	S2o	1.44(10)	$E2$	
6947.3	1214.8	7(2)	$18^+ \to 16^+$	S2o	1.44(10)	$E2$	
	446		$18^+ \to 17^+$	D1		$M1/E2$	
S2o′							
4155.3	877.6	3(1)	$11^+ \to 9^+$	t band	1.54(17)	$E2$	
	730.7	7(1)	$11^+ \to 10^+$	S2o	0.12(6)	$M1/E2$	
4870.9	879.7	4(1)	$13^+ \to 12^+$	S2o	0.76(27)	$M1/E2$	
	716.7	3(1)	$13^+ \to 11^+$	S2o′	1.66(55)	$E2$	
5723.0	937.8	8(2)	$15^+ \to 14^+$	S2o	0.17(5)	$M1/E2$	
	(852)		$15^+ \to 13^+$	S2o′		$E2$	
6840	1107	3(1)	$17^+ \to 16^+$	S2o	0.88(13)	$M1/E2$	
	1117		$17^+ \to 15^+$	S2o′		$E2$	
S2″							
6650.7	918.2	17(4)	$18^+ \to 16^+$	S2o	1.53(6)	$E2$	
7579.0	928.2	10(3)	$20^+ \to 18^+$	S2″	1.33(8)	$E2$	
8666.7	1087.7	6(1)	$(22^+) \to 20^+$	S2″		$E2$	
9913.3	1246.6		$(24^+) \to (22^+)$	S2″		$E2$	
(11327)	(1414)		$(26^+) \to (24^+)$	S2″		$E2$	
S2p							
5086.3	861.8	31(8)	$(14^+) \to 12^+$	GSB			
6046.3	960.0	3(1)	$(16^+) \to (14^+)$	S2p			
7136.2	1089.9		$(18^+) \to (16^+)$	S2p			
N1 band							
1918.3	1561.2		$3^- \to 2^+$	GSB		$E1$	
	1016.7		$3^- \to 4^+$	GSB		$E1$	
2169.1	250.8		$5^- \to 3^-$	N1		$E2$	
	1267.4	81(3)	$5^- \to 4^+$	GSB	0.78(4)	$E1$	
	575.9	51(9)	$5^- \to 6^+$	GSB	0.96(3)	$E1$	
	691.8		$5^- \to 4^+$	γ band		$E1$	
2569.1	400.0	86(3)	$7^- \to 5^-$	N1	1.41(7)	$E2$	
	467.4	15(1)	$7^- \to 6^+$	γ band	0.76(4)	$E1$	
	975.9	237(8)	$7^- \to 6^+$	GSB	0.80(3)	$E1$	
	173.2	8(1)	$7^- \to 8^+$	GSB	0.86(6)	$E1$	
3068.2	499.0	219(7)	$9^- \to 7^-$	N1	1.37(5)	$E2$	
	138.1	2(2)	$9^- \to 8^-$	N2	0.57(3)	$M1/E2$	−0.16(5)
	672.0	47(6)	$9^- \to 8^+$	GSB	0.93(10)	$E1$	

TABLE I. (*Continued.*)

E_i (level)	E_γ (keV)	T_γ	$I_i^\pi \to I_f^\pi$	Final state band	R_{ac} ratio	Mult.	δ
3769.8	701.7	5(2)	$10^- \to 9^-$	N1		$M1/E2$	
	443.8	2(1)	$10^- \to 9^-$	N2		$M1/E2$	
	592.2	2(1)	$10^- \to 8^-$	F5		$E2$	
	839.8	3(1)	$10^- \to 8^-$	N2		$E2$	
	334.2	4(1)	$10^- \to 10^-$	N2	1.44(19)	$M1/E2$	
3660.3	224.1	6(1)	$11^- \to 10^-$	N2	0.51(9)	$M1/E2$	$-0.23(10)$
	592.2	183(14)	$11^- \to 9^-$	N1	1.76(4)	$E2$	
4436.6	666.8	6(2)	$12^- \to 10^-$	N1	1.67(24)	$E2$	
	776.7	5(1)	$12^- \to 11^-$	N1		$M1/E2$	
	(608)		$12^- \to 10^-$	F5			
4355.8	276.4	$\leqslant 6$	$13^- \to 12^-$	N2	0.39(10)	$M1/E2$	$-0.31(13)$
	695.5	158(18)	$13^- \to 11^-$	N1	1.68(8)	$E2$	
5222.7	786.1	11(2)	$14^- \to 12^-$	N1	1.32(20)	$E2$	
	865.7	2(1)	$14^- \to 13^-$	N1		$M1/E2$	
5157.6	276.5		$15^- \to 14^-$	N2	0.39(10)	$M1/E2$	$-0.31(13)$
	801.8	134(15)	$15^- \to 13^-$	N1	1.53(7)	$E2$	
6076.2	853.5	6(2)	$16^- \to 14^-$	N1	1.63(13)	$E2$	
	919.2		$16^- \to 15^-$	N1		$M1/E2$	
6039.8	882.3	65(9)	$17^- \to 15^-$	N2	1.60(5)	$E2$	
6949.7	873.5	2(1)	$18^- \to 16^-$	N1	1.69(15)	$E2$	
6974.9	935.0	48(5)	$19^- \to 17^-$	N1	1.44(16)	$E2$	
7953.6	978.7	18(2)	$21^- \to 19^-$	N1	1.07 (7)	$E2$	
9005.5	1051.9	17(2)	$23^- \to 21^-$	N1	1.77(17)	$E2$	
10155.9	1150.5	6(1)	$(25^-) \to 23^-$	N1		$E2$	
11419	1263		$(27^-) \to (25^-)$	N1		$E2$	
N2 band							
2511.0	341.9	4(1)	$(6^-) \to 5^-$	N1			
2930.6	419	2(1)	$8^- \to (6^-)$	N2			
	360.9	88(8)	$8^- \to 7^-$	N1	0.72(4)	$M1/E2$	$-0.02(5)$
	140.4	2(1)	$8^- \to 7^-$	F5	0.39(11)	$M1/E2$	
3326.2	396.2	10(2)	$9^- \to 8^-$	N2	0.50(5)	$M1/E2$	
	257.8	2(1)	$9^- \to 9^-$	N1	1.11(13)	$M1/E2$	
	757.6		$9^- \to 7^-$	N1		$E2$	
3436.3	506.3	50(4)	$10^- \to 8^-$	N2	1.38(5)	$E2$	
	367.7	40(3)	$10^- \to 9^-$	N1	0.75(2)	$M1/E2$	$-0.02(4)$
3944.2	617.6	4(1)	$11^- \to 9^-$	N2	1.51(12)	$E2$	
	507.9	5(2)	$11^- \to 10^-$	N2	1.02(9)	$M1/E2$	
4079.4	643.1	75(7)	$12^- \to 10^-$	N2	1.43(5)	$E2$	
	418.9	3(1)	$12^- \to 11^-$	N1	0.56(6)	$M1/E2$	$-0.19(7)$
4727	783.8	12(2)	$13^- \to 11^-$	N2	1.57(22)	$E2$	
	647.8	3(1)	$13^- \to 12^-$	N1		$M1/E2$	
4881.2	801.9	71(1)	$14^- \to 12^-$	N2	1.53(7)	$E2$	
	524.5	12(2)	$14^- \to 13^-$	N1	0.37(5)	$M1/E2$	$-0.47(13)$
5601.8	874.9	10(3)	$(15^-) \to 13^-$	N2			
	720.5	4(1)	$(15^-) \to 14^-$	N2			
5769.1	887.9	45(3)	$16^- \to 14^-$	N2	1.34(7)	$E2$	
	611.4	11(2)	$16^- \to 15^-$	N1		$M1/E2$	
6534	932	5(2)	$(17^-) \to (15^-)$	N2			
6720.0	950.9	25(4)	$18^- \to 16^-$	N2	1.78(25)	$E2$	
	679.8		$18^- \to 17^-$	N1		$M1/E2$	
7718.7	998.7	8(2)	$20^- \to 18^-$	N2	1.78(27)	$E2$	
To N2							
5099.0	1019.6	6(3)	$14^- \to 12^-$	N2	1.11(13)	$E2$	
N3							
2238.2	1336.4	8(1)	$5^- \to 4^+$	GSB	0.95(6)	$E1$	
2529.1	291.2	4(1)	$6^- \to 5^-$	N3	0.82(9)	$M1/E2$	
	251.4	9(2)	$6^- \to 5^-$	N4	0.41(3)	$M1/E2$	
	516.3	10(2)	$6^- \to 5^+$	γ band		$E1$	

TABLE I. (*Continued.*)

E_i (level)	E_γ (keV)	T_γ	$I_i^\pi \to I_f^\pi$	Final state band	R_{ac} ratio	Mult.	δ
2851.0	573.7	8(2)	$7^- \to 5^-$	N4	1.63(15)	$E2$	
	612.9	3(1)	$7^- \to 5^-$	N3		$E2$	
	322.3		$7^- \to 6^-$	N3		$M1/E2$	
3090.0	560.9	14(4)	$8^- \to 6^-$	N3	1.62(27)	$E2$	
	388.1	7(1)	$8^- \to 7^-$	N4		$M1/E2$	
3498	647	3(1)	$(9^-) \to 7^-$	N3			
3790.6	700.6	17(6)	$10^- \to 8^-$	N3	1.21(27)	$E2$	
4311	813	2(1)	$(11^-) \to (9^-)$	N3			
4617.1	826.5	7(3)	$(12^-) \to 10^-$	N3			
5182	871	2(1)	$(13^-) \to (11^-)$	N3			
5549	932	3(2)	$(14^-) \to (12^-)$	N3			
N4							
2277.3	1375.5	20(2)	$5^- \to 4^+$	GSB	0.82(4)	$E1$	
2701.7	424.1	15(3)	$7^- \to 5^-$	N4	1.75(10)	$E2$	
	172.7	3(1)	$7^- \to 6^-$	N3		$M1/E2$	
	1108.5	14(3)	$7^- \to 6^+$	GSB	0.78(5)	$E1$	
	598.8	15(5)	$7^- \to 6^+$	γ band	0.73(7)	$E1$	
3291.4	589.7	18(7)	$9^- \to 7^-$	N4	1.62(27)	$E2$	
4037.5	746.1	17(7)	$(11^-) \to 9^-$	N4			
4905	867.5	$\leqslant 4$	$(13^-) \to (11^-)$	N4			
N5							
2866.9	391.8	$\geqslant 80$	$9^- \to 8^-$	N5	0.27(3)	$M1/E2$	$-0.81(48)$
3317.4	450.5	50(3)	$10^- \to 9^-$	N5	0.31(3)	$M1/E2$	$-0.60(15)$
	842.6	19(5)	$10^- \to 8^-$	N5	1.16(16)	$E2$	
3781.9	464.5	42(3)	$11^- \to 10^-$	N5	0.41(2)	$M1/E2$	$-0.37(6)$
	915.5	30(2)	$11^- \to 9^-$	N5	1.54(17)	$E2$	
4299.2	517.7	35(5)	$12^- \to 11^-$	N5	0.42(3)	$M1/E2$	$-0.39(7)$
	982.5	30(3)	$12^- \to 10^-$	N5	1.53(10)	$E2$	
4770.9	471.7	18(5)	$13^- \to 12^-$	N5	0.41(5)	$M1/E2$	$-0.37(13)$
	989.8	36(3)	$13^- \to 11^-$	N5	1.48(8)	$E2$	
5349.9	578.1	3(1)	$14^- \to 13^-$	N5	0.37(9))	$M1/E2$	
	1050.7	16(5)	$14^- \to 12^-$	N5	1.61(34)	$E2$	
5836.3	486		$(15^-) \to 14^-$	N5			
	1065.4		$(15^-) \to 13^-$	N5			
	933.7		$(15^-) \to 13^-$	F6			
To N5							
5406.7	1109.2	12(2)	$14^- \to 12^-$		1.52(27)	$E2$	
	635.8	12(2)	$14^- \to 13^-$			$M1/E2$	
N6							
5452.4	681.1	8(1)	$14^- \to 13^-$	N5	0.86(21)	$M1/E2$	
	1153.2	10(2)	$14^- \to 12^-$	N5	1.19(18)	$E2$	
5713.8	363.3		$15^- \to 14^-$	N5		$M1/E2$	
	942.9	16(2)	$15^- \to 13^-$	N5	1.49(18)	$E2$	
6088.3	637.6	13(2)	$16^- \to 14^-$	N6	1.55(22)	$E2$	
	681.6		$16^- \to 14^-$			$E2$	
6587.5	873.7	10(1)	$17^- \to 15^-$	N6	1.74(23)	$E2$	
6901.2	812.9	10(2)	$18^- \to 16^-$	N6	1.93(29)	$E2$	
7561.1	973.6	4(2)	$(19^-) \to 17^-$	N6			
7924.3	1023.1	8(1)	$(20^-) \to 18^-$	N6			
t **band**							
2982.7	182.1	2(2)	$8^+ \to 8^+$	γ band	1.77(13)	$M1/E2$	
	587.1		$8^+ \to 8^+$	GSB		$M1/E2$	
	507.6	18(2)	$8^+ \to 8^-$	N5	1.48(5)	$E1$	
3277.5	294.8	27(2)	$9^+ \to 8^+$	*t* band	0.45(2)	$M1/E2$	$-0.30(5)$
	802.2		$9^+ \to 8^-$	N5		$E1$	
3762.0	484.5	6(1)	$10^+ \to 9^+$	*t* band	0.63(4)	$M1/E2$	$-0.12(5)$
	779.3	5(1)	$10^+ \to 8^+$	*t* band		$E2$	

TABLE I. (*Continued.*)

E_i (level)	E_γ (keV)	T_γ	$I_i^\pi \rightarrow I_f^\pi$	Final state band	R_{ac} ratio	Mult.	δ
3963.9	(202)		$11^+ \rightarrow 10^+$	t band		$M1/E2$	
	686.4	6(2)	$11^+ \rightarrow 9^+$	t band	1.42(12)	$E2$	
	539.4	21(5)	$11^+ \rightarrow 10^+$	S2o	0.38(4)	$M1/E2$	$-0.53(14)$
4405.2	441.3	9(2)	$12^+ \rightarrow 11^+$	t band	0.40(4)	$M1/E2$	$-0.38(8)$
	643.0	2(1)	$12^+ \rightarrow 10^+$	t band		$E2$	
	980.8	6(2)	$12^+ \rightarrow 10^+$	S2o	1.36(20)	$E2$	
	1144.0	11(3)	$12^+ \rightarrow 10^+$	GSB	1.35(20)	$E2$	
4796	(391)		$13^+ \rightarrow 12^+$	t band		$M1/E2$	
	832	13(3)	$13^+ \rightarrow 11^+$	t band	2.0(10)	$E2$	
D1 band							
4910.5	453		$12^+ \rightarrow 11^+$	S1$'$		$M1/E2$	
	1306		$12^+ \rightarrow 10^+$	γ band		$E2$	
	1649		$12^+ \rightarrow 10^+$	GSB		$E2$	
5166.2	255.7	$\geqslant 4$	$13^+ \rightarrow 12^+$	D1	0.34(7)	$M1/E2$	$-0.52(24)$
	457.9		$13^+ \rightarrow (12^+)$	F2		$M1/E2$	
	760.1		$13^+ \rightarrow 12^+$	t band		$M1/E2$	
5443.0	276.8	$\geqslant 3$	$14^+ \rightarrow 13^+$	D1	0.52(5)	$M1/E2$	$-0.22(7)$
	289.7	$\geqslant 2$	$14^+ \rightarrow 13^+$	D1	0.43(4)	$M1/E2$	$-0.35(8)$
5762.1	319.1	6(2)	$15^+ \rightarrow 14^+$	D1	0.59(4)	$M1/E2$	$-0.16(5)$
	268.3	3(2)	$15^+ \rightarrow 14^+$	F2	0.36(5)	$M1/E2$	$-0.47(14)$
	977.4	2(1)	$15^+ \rightarrow 14^+$	S2o	0.47(6)	$M1/E2$	
6111.1	349.0	11(1)	$16^+ \rightarrow 15^+$	D1	0.56(4)	$M1/E2$	$-0.19(5)$
6500.3	389.2	9(3)	$17^+ \rightarrow 16^+$	D1	0.53(4)	$M1/E2$	$-0.23(7)$
6934.1	433.5	4(2)	$18^+ \rightarrow 17^+$	D1	0.41(9)	$M1/E2$	-0.26
	1201.6	6(2)	$18^+ \rightarrow 16^+$	S2o	1.67(20)	$E2$	
7419.9	485.6		$19^+ \rightarrow 18^+$	D1		$M1/E2$	$-0.30(10)$
	919.6	2(1)	$19^+ \rightarrow 17^+$	D1		$E2$	
	472.7		$19^+ \rightarrow 18^+$	S2o		$M1/E2$	
7926	505.5		$(20^+) \rightarrow 19^+$	D1			
D2 band							
5960.6	1079.4	10(3)	$15^- \rightarrow 14^-$	N2	0.86(12)	$M1/E2$	
	737.8		$15^- \rightarrow 14^-$	N1		$M1/E2$	
6218.1	257.5		$16^- \rightarrow 15^-$	D2		$M1/E2$	
	1060.5	7(1)	$16^- \rightarrow 15^-$	N1	0.24(12)	$M1/E2$	
	894.6	3(1)	$16^- \rightarrow 14^-$	F4		$E2$	
6498.3	280.2	2(1)	$17^- \rightarrow 16^-$	D2	0.70(9)	$M1/E2$	
	340.9	4(1)	$17^- \rightarrow 16^-$	F4	0.58(12)	$M1/E2$	
6914.5	416.2		$(18^-) \rightarrow 17^-$	D2			
7335	420		$(19^-) \rightarrow (18^-)$	D2			
7849	514		$(20^-) \rightarrow (19^-)$	D2			
F1							
889	532		$\rightarrow 2^+$	GSB			
1545	656			F1			
2231	686			F1			
2342	111			F1			
F2							
4706.7	742.8	3(1)	$(12^+) \rightarrow 11^+$	t band			
	553	2(1)	$(12^+) \rightarrow 11^+$	S2o$'$			
	945.2		$(12^+) \rightarrow 10^+$	t band			
5153.3	446		$13^+ \rightarrow (12^+)$	F2			
	748.1	2(1)	$13^+ \rightarrow 12^+$	t band	0.53(23)	$M1/E2$	
5493.8	(341)		$14^+ \rightarrow 13^+$	F2		$M1/E2$	
	327.9		$14^+ \rightarrow 13^+$	D1		$M1/E2$	
	698.4		$14^+ \rightarrow 13^+$	t band		$M1/E2$	
F3							
3902	624	4(1)	$10^+ \rightarrow 9^+$	t band	0.49(4)	$M1/E2$	$-0.26(7)$
4580	678	2(1)	$\rightarrow 10^+$	F3			

TABLE I. (*Continued.*)

E_i (level)	E_γ (keV)	T_γ	$I_i^\pi \to I_f^\pi$	Final state band	R_{ac} ratio	Mult.	δ
F4							
5323.5	967.7	11(4)	$14^- \to 13^-$	N1	0.31(10)	$M1/E2$	
6157.4	833.2	4(2)	$16^- \to 14^-$	F4		$E2$	
	999.8	16(2)	$16^- \to 15^-$	N1	0.18(7)	$M1/E2$	
F5							
2789.8	1196.6	17(2)	$7^- \to 6^+$	GSB	0.87(10)	$E1$	
	688.2		$7^- \to 6^+$	γ band			
3176.7	386.9	9(5)	$8^- \to 7^-$	F5	0.51(7)	$M1/E2$	
	(608)		$8^- \to 7^-$	N1			
3828.1	501.9	5(1)	$10^- \to 9^-$	N2			
	651.6		$10^- \to 8^-$	F5			
F6							
4036.0	718.6	2(1)	$11^- \to 10^-$	N5	0.36(9)	$M1/E2$	
4616.4	1299.0	4(1)	$11^- \to 10^-$	N5	0.86(24)	$M1/E2$	
4902.8	866.8		$13^- \to 11^-$	F6		$E2$	
	603.6	8(2)	$13^- \to 12^-$	N5	0.56(18)	$M1/E2$	
	1121		$13^- \to 11^-$	N5		$E2$	
4882	266		$\to 11^-$	F6			
5945	1042		$(15^-) \to 13^-$	F6			

Band S1 was first reported up to 16^+ in Ref. [23], and extended to 20^+ in Ref. [28]. However, the uppermost 928-keV transition is not observed in double-gated spectra in the present work [see Fig. 2(d)]. The existence of this transition was supported by a summed spectrum gated on the 629- and 794-keV transitions [28]. However, there is another 794-keV transition in band S2o and a newly identified 928-keV transition in band S2″ which are in coincidence [see Fig. 2(f)]. Therefore we removed this transition from band S1.

Band S2o was reported up to 18^+ in Ref. [23], and extended to 20^+ in Ref. [28]. However, the uppermost two transitions (1027 and 1040 keV) are not observed in double-gated spectra in the present work [see Fig. 2(f)]. For these two transitions, only one spectrum gated on the 730-keV transition was published, supporting the existence of the 1027-keV transition. However, the peak at 1027 keV was very weak, and it may come from the contamination by the 1029-keV transition linking band S2o to GSB, which is in coincidence with a newly identified 731-keV in-band transition. These two transitions have been removed.

Two transitions at 590 and 746 keV in band N4 and one at 1108 keV deexciting band N4 have been reported previously, but placed differently. According to the double-gated spectra [see Fig. 2(s)], their locations have been changed.

IV. DISCUSSION

In this paper the discussion focuses on the negative-parity bands (N1–N6 and D2) since most of the positive-parity bands have been discussed in Ref. [29]. Among them, parts of bands N1 and N2 were previously reported in Refs. [23,25,28]. Bands N5 and N6, which are built on a well-known K-isomer, were recently discussed in our two foregoing papers [17,29]. The excitation energies of the seven negative-parity bands are shown in Fig. 3.

To assign the configurations of the two-quasiparticle bands N1–N5, their alignments are shown in Fig. 4, in comparison with the single-quasiparticle bands in the neighboring ^{129}Cs and ^{129}Ba nuclei. In ^{130}Ba, a diversity of shapes has been revealed, therefore it is impossible to find a set of Harris parameters suitable for all the bands. In Fig. 4, two sets of Harris parameters are used, with different $\mathcal{J}_1$ values which have more influence on the states with higher spins. In this region, the first band crossing is mainly caused by the alignment of either a $\pi h_{11/2}$ proton pair or a $\nu h_{11/2}$ neutron pair. Usually the proton alignment is expected to occur much earlier ($\hbar\omega = 0.30$–0.35 MeV) than the neutron alignment ($\hbar\omega > 0.4$ MeV) [51], excepting the configurations with one quasiproton in the $\pi h_{11/2}$ orbital which blocks the proton alignment. Two extra quasiprotons in the $\pi h_{11/2}$ orbital are expected to drive the nuclei to a larger deformation. Therefore a larger $\mathcal{J}_1$ is adopted for all the bands, except those involving quasiprotons occupying the $\pi h_{11/2}$ orbital.
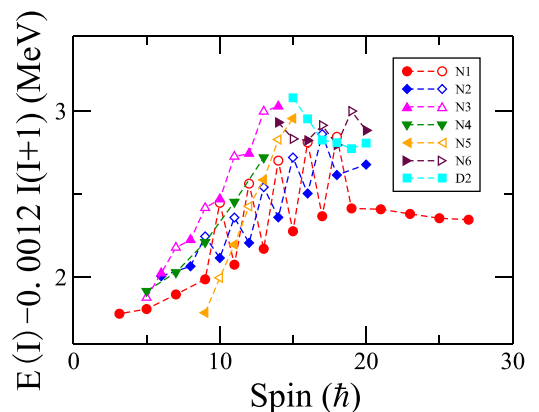

FIG. 3. The excitation energies of observed negative-parity bands of ^{130}Ba are shown relative to a rotating rigid rotor reference.
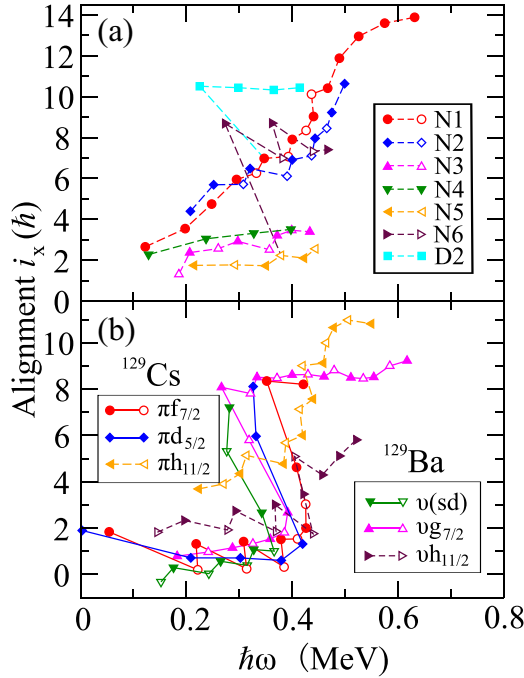
FIG. 4. Experimental quasiparticle alignments as a function of rotational frequency for the negative-parity bands of ^{130}Ba are shown in the upper panel, while those for bands in ^{129}Cs and ^{129}Ba are shown in the lower panel. The Harris parameters used for bands N1–N4, D2, and $\pi h_{11/2}$ in ^{129}Cs are $\mathcal{J}_0 = 14 \ \hbar^2 \text{MeV}^{-1}$ and $\mathcal{J}_1 = 15 \ \hbar^4 \text{MeV}^{-3}$, while for the other bands they are $\mathcal{J}_0 = 14 \ \hbar^2 \text{MeV}^{-1}$ and $\mathcal{J}_1 = 38 \ \hbar^4 \text{MeV}^{-3}$.

Considering that these single-particle orbitals are identified in ^{129}Cs and ^{129}Ba, the possible configurations for negative-parity two-quasiparticle bands in ^{130}Ba are $\pi h_{11/2}(g_{7/2}, d_{5/2})$, $\nu h_{11/2}g_{7/2}$, and $\nu h_{11/2}(s_{1/2}, d_{3/2})$. Band N5 built on the K isomer was assigned to the configuration $\nu h_{11/2}g_{7/2}$ in Ref. [17]. The alignments of bands N1 and N2 ($\approx 5\hbar$) are significantly larger than those of bands N3 and N4 ($\approx 2\hbar$), leading to an assignment of $\pi h_{11/2}(g_{7/2}, d_{5/2})$ to the former and $\nu h_{11/2}(s_{1/2}, d_{3/2})$ to the latter. The assignment for bands N1 and N2 is in agreement with Sun *et al.* [25], who suggested the previously known structure to be built on the $\pi h_{11/2}d_{5/2}$ or $\pi h_{11/2}g_{7/2}$ configurations according to the Routhian calculation and signature splitting analysis. In the present work, two transitions at 598 and 723 keV have been identified, linking band S1 to band N1 [see Fig. 2(q)]. Since the configuration of band S1 is $\pi h_{11/2}^2$, the existence of these two transitions further supports the assignment of two-quasiproton configuration.

1. Bands N1, N2, and D2

In the previous works, the favored signature branches of bands N1 and N2 were regarded as the two signature branches of the same configuration. However, two newly observed extra branches extend the structure to a set of four branches which are grouped in two rotational bands built on the $\pi h_{11/2}(g_{7/2}, d_{5/2})$ configuration. The two new branches are located far way from the yrast line compared to the two

previously known branches, and therefore are weakly populated. The favored signature branches with configurations dominated by $\pi h_{11/2}g_{7/2}$ and $\pi h_{11/2}d_{5/2}$ are expected to have odd and even spins, respectively. Therefore, it is straightforward to assign the most yrast odd-spin branch to the favored signature of the $\pi h_{11/2}g_{7/2}$ configuration, and the yrare odd-spin branch to the unfavored signature of the $\pi h_{11/2}d_{5/2}$ configuration. However, it is not easy to assign the other two branches to the $\pi h_{11/2}g_{7/2}$ or the $\pi h_{11/2}d_{5/2}$ configurations.

Actually, similar structures have been discussed in the neighboring cesium isotopes ^{125,127,129}Cs [7,12]. In each of these nuclei, three branches were found built on the $\pi (g_{7/2}, d_{5/2})$ configurations. Among them, more intense linking transitions were found between the two yrast branches, which were regarded as signature partners in earlier studies. However, strong admixture of wave functions is expected between the close-lying pseudospin partners $\pi g_{7/2}$ and $\pi d_{5/2}$, and thus the observation of intense linking transitions do not, *a priori*, implicate a signature pair. In fact, two such branches have been reinterpreted as the favored signature branches of the pseudospin partner bands based on a convincing discussion involving signature splitting and the decay pattern at low spins [7].

To compare bands N1 and N2 with the neighboring cesium isotopes, we plot their signature and pseudospin splittings in Fig. 5. The signature splitting is defined as $[E(I) - E_{sp}(I-1)] - [E_{sp}(I+1) - E(I) + E_{sp}(I-1) - E(I-2)]/2$, while the pseudospin splitting is defined accordingly as $[E(I) - E_{pp}(I-1)] - [E_{pp}(I+1) - E(I) + E_{pp}(I-1) - E(I-2)]/2$. Here $E_{sp}(I)$ means the level energy of the state with spin I in the signature partner branch, and $E_{pp}(I)$ means the level energy in the pseudospin partner band. In bands N1 and N2, one quasiproton occupies the low-Ω $\pi h_{11/2}[550]1/2^+$ orbital, which induces a large signature splitting. One therefore expects signature splittings of the two bands similar to those of the corresponding single-quasiproton $\pi (g_{7/2}, d_{5/2})$ bands in the neighboring odd-A nuclei. As for the pseudospin splitting, which can be attributed to the difference in excitation energies between two pseudospin partner orbitals, it should not change significantly by the coupling of another proton in the $\pi h_{11/2}$ orbital. In Fig. 5, we consider band N1 as one signature pair built on $\pi h_{11/2}g_{7/2}$, and band N2 as another signature pair built on $\pi h_{11/2}d_{5/2}$. With such assignments, the signature splitting of band N1 has an amplitude simiar to those of $\pi g_{7/2}$ bands in Cs isotopes, while the pseudospin splitting between bands N1 and N2 is also similar to those between $\pi g_{7/2}$ and $\pi d_{5/2}$ bands in ^{125,127,129}Cs. Alternatively, if we regard the two yrast branches in bands N1 and N2 as a signature pair, the signature and pseudospin splittings in Fig. 5 should change, both being inconsistent with those in the cesium isotopes. The similar patterns of the splittings indicate that bands N1 and N2 are built on the $\pi h_{11/2}g_{7/2}$ and $\pi h_{11/2}d_{5/2}$ configurations, respectively. The low-spin pseudospin crossing in the cesium isotopes are not observed in ^{130}Ba. In fact, the crossing in cesium isotopes occurs at a rotational frequency $\hbar\omega \approx 0.1$ MeV [7], while band N2 of ^{130}Ba starts at $\hbar\omega \approx 0.2$ MeV. Therefore such a crossing, if it exists in ^{130}Ba, would be beyond the observation in this experiment. In the neighboring barium isotopes ^{126,128}Ba
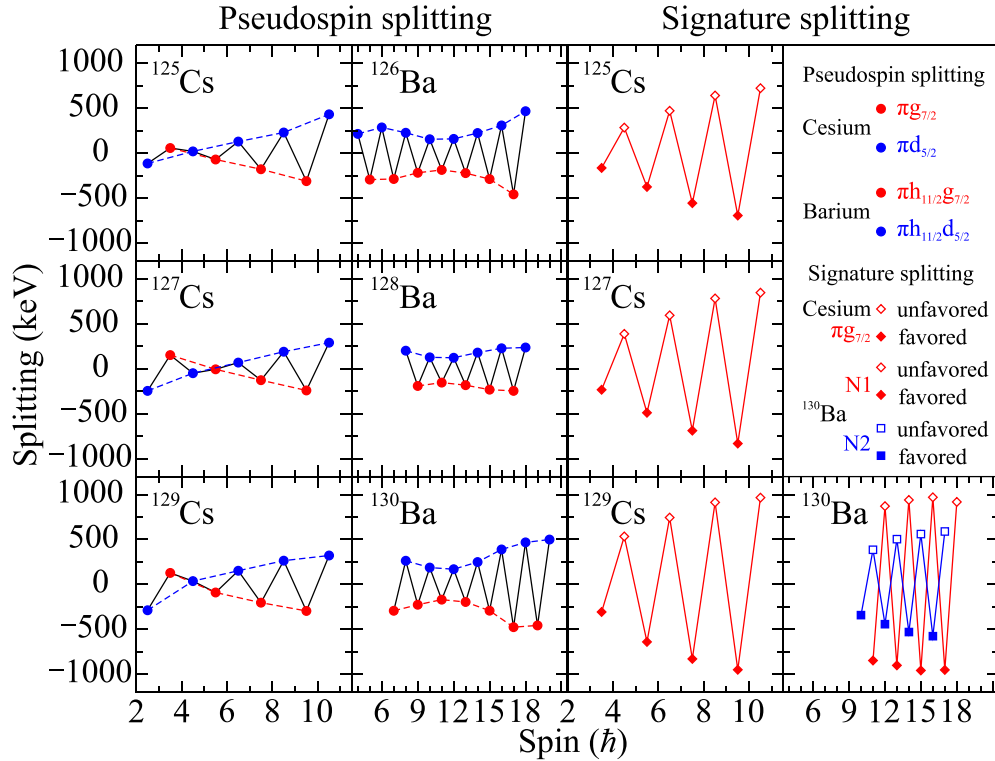
FIG. 5. The signature and pseudospin splittings of bands built on the $\pi(g_{7/2}, d_{5/2})$ configurations in ^{125,127,129}Cs and those built on the $\pi h_{11/2} \otimes \pi(g_{7/2}, d_{5/2})$ configurations in ^{126,128,130}Ba.

[52,53], two branches have been reported and interpreted as a signature pair built on $\pi h_{11/2}g_{7/2}$ or $\pi h_{11/2}d_{5/2}$ configuration in each nuclei. However, according to the systematics, they are also more likely to be the signature favored branches of pseudospin partner bands.

The present assignments for bands N1 and N2 is further supported by the decay pattern of the odd-spin branch of N2 which is the unfavored signature branch of the $\pi h_{11/2}d_{5/2}$ configuration. Except for its bandhead, no transitions feeding to the two branches of band N1 have been found. With the present assignments, it is reasonable that only the intraband transitions are observed. However, if the even-spin branch of N2 is regarded as the unfavored signature branch of the $\pi h_{11/2}g_{7/2}$ configuration assigned to band N1, it should be anomalous that no $E2$ transitions with much larger transition energy are observed to the favored signature branch, while the decay routes are dominated by $E2$ transitions in the whole structure. Moreover, the intraband transitions to the odd-spin branch of band N1 are also expected with such assignments, but not observed.

It is also useful to compare the data with projected shell model (PSM) calculations. A deformed basis is necessary for such a calculation. As suggested in Ref. [54], the quadrupole $\epsilon_2 = 0.22$ and hexadecapole $\epsilon_4 = 0.02$ deformations are adopted. The monopole-pairing strength is taken to be $G_M = [20.82 \pm 13.58(N - Z)/A]/A$, for protons and neutrons, respectively. The quadrupole-pairing strength G_Q is assumed to be proportional to G_M, with the proportionality constant 0.18 for ^{130}Ba. For the valence single-particle space, we include three major shells, $N = 3$, 4, and 5, for both

neutrons and protons. For the present PSM calculations, it is not feasible to extract the theoretical errors.

The PSM results after configuration mixing are compared with the experimental data. The experimental and calculated excitation energies are plotted in Fig. 6. In general, the calculated energies are slightly higher than the experimental ones, and the difference increases gradually with increasing spin. It appears that the used deformation parameters, which were deduced for the ground state, can be a bit different from those in the two-quasiparticle bands. In fact, the deformation for bands N1 and N2 could be larger, since the $\pi h_{11/2}$ and $\pi(g_{7/2}, d_{5/2})$ orbitals get closer with increasing deformation. The signature splitting of band N1 is well reproduced, while
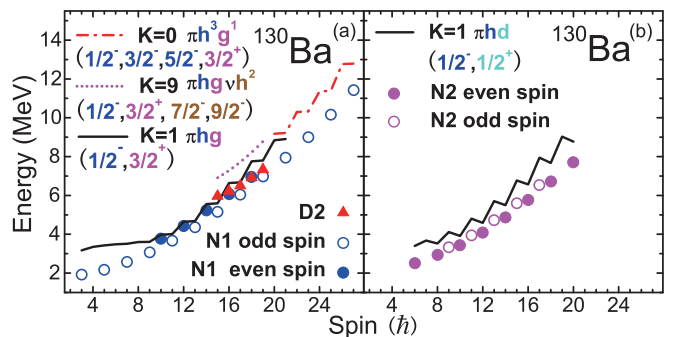

FIG. 6. Excitation energies obtained by PSM in comparison with the experimental data for bands N1, N2, and D2 (left panel) and for bands N3 and N4 (right panel).
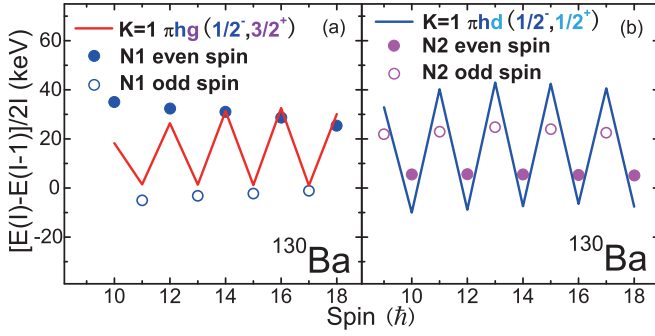
FIG. 7. Signature splitting obtained by PSM in comparison with the experimental data for bands N1 (left panel) and N2 (right panel).
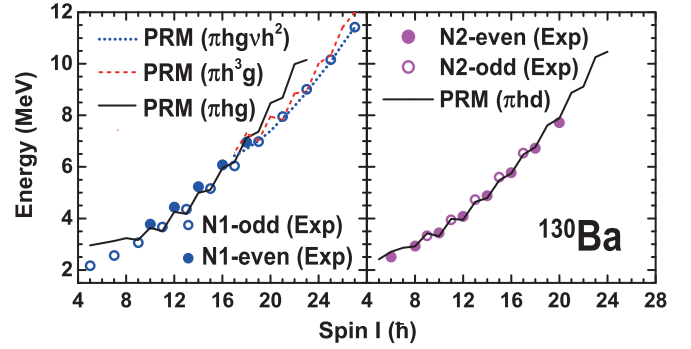

FIG. 9. Excitation energies obtained by PRM in comparison with the experimental data for band N1 (left panel) and for band N2 (right panel).

that of N2 is larger than experimental data (see Fig. 7). The signature splitting can be considerably affected by the triaxial deformation. A further calculation using the triaxial projected shell model (TPSM) is expected to reduce the discrepancy between experimental and theoretical energies. The theoretical $B(M1)/B(E2)$ ratios are in good agreement with the available experimental data for bands N1 and N2 (see Fig. 8).

A band crossing has been identified in the odd-spin branch of band N1 with a frequency $\omega \approx 0.42$ MeV/$\hbar$. Two possible scenarios for this alignment are the band crossings induced by a $\pi h_{11/2}$ proton pair and a $\nu h_{11/2}$ neutron pair. For the $\pi h_{11/2}$ band in neighboring ^{129}Cs, the observed band crossing has been suggested to originate from a $\nu h_{11/2}$ pair since the breaking of a $\pi h_{11/2}$ pair is expected to be delayed by the blocking effect [12]. In fact, the crossing frequency for a blocked proton has been estimated to be larger than 0.5 MeV/$\hbar$ by Hildingsson *et al.* [51] using the Total Routhian Surfaces calculations with universal Woods-Saxon potential. Similarly, the bands built on the $\pi h_{11/2}(g_{7/2}, d_{5/2})$ configuration in ^{128}Ba [53] and ^{132}Ba [55] have also been explained as being crossed by a four-quasiparticle configuration containing another aligned $\nu h_{11/2}$ pair. In ^{132}Ce, the alignment for the corresponding band has been interpreted to be the combination of two consecutive band crossings of both $\pi h_{11/2}$ and $\nu h_{11/2}$ pairs [56]. However, the alignment of the corresponding band in ^{136}Nd was

interpreted to originate from the band crossing induced by a $\pi h_{11/2}$ pair [57].

Before the band crossing, the alignment increases gradually, which can be flattened only by assuming a set of unreasonably large Harris parameters. This could be caused by the octupole correlation between the $\pi h_{11/2}$ and $\pi d_{5/2}$ orbitals, which is significant in barium nuclei.

In the PSM calculations for bands N1 and N2, the triaxial deformation degrees of freedom are not taken into account. To check the effects of the triaxial deformation, we performed particle rotor model (PRM) [39,58–61] calculations. The deformation parameters of the configuration $\pi h_{11/2}(g_{7/2}, d_{5/2})$ are $\beta = 0.23$ and $\gamma = 19.6°$ according to the configuration-fixed covariant density functional theory (CDFT) [62,63] calculation with PC-PK1 effective interaction [64]. Using the same deformation parameters, PRM calculations are carried out for the low spin part of band N1 with the configuration $\pi h_{11/2}g_{7/2}$ and for band N2 with the configuration $\pi h_{11/2}d_{5/2}$. For the moments of inertia, the irrotational type $\mathcal{J}_k = \mathcal{J}_0 \sin^2(\gamma - 2k\pi/3)$ is adopted, with $\mathcal{J}_0 = 23.0$ $\hbar^2$/MeV for band N1 and $\mathcal{J}_0 = 30.0$ $\hbar^2$/MeV for band N2. For the present PRM calculations, it is not feasible to extract the theoretical errors.

The obtained energy spectra and corresponding signature splitting for bands N1 and N2 are shown in Figs. 9 and 10,

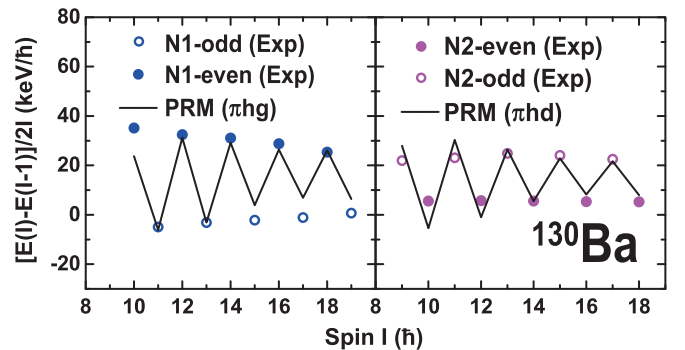FIG. 8. $B(M1)/B(E2)$ ratios obtained by PSM in comparison with the experimental data for bands N1 and N2.

FIG. 10. Signature splitting obtained by PRM in comparison with the experimental data for band N1 (left panel) and for band N2 (right panel).

respectively. The PRM can reproduce the experimental energy spectra, which further confirms the configuration assignments for these two bands. In comparison with asymmetric PSM, PRM with triaxial deformation shapes has improved a bit the descriptions of the signature splitting for bands N1 and N2. In particular, the overestimated signature splitting for band N2 in the PSM calculations has been reduced in the PRM calculations, which justifies the importance of the triaxial deformation.

For the high spin part of band N1, we present the results of energy spectra calculated by PRM with configurations $\pi h_{11/2}^3 g_{7/2}$ and $\pi h_{11/2} g_{7/2} \nu h_{11/2}^{-2}$ in Fig. 9. For the former one, the deformation parameters are $\beta = 0.24$ and $\gamma = 18.5°$ according to the CDFT calculations, and the used moment of inertia is $\mathcal{J}_0 = 26.0 \, \hbar^2/\mathrm{MeV}$. For the latter one, the obtained deformation parameters are $\beta = 0.22$ and $\gamma = 22.4°$, and $\mathcal{J}_0 = 22.0 \, \hbar^2/\mathrm{MeV}$ is used. Both configurations can reproduce the high spin part of band N1. Since the valence particle favors alignment along the short axis and the valence hole favors alignment along the long axis, the configuration $\pi h_{11/2}^3 g_{7/2}$ gives two $\Delta I = 2$ bands whereas the configuration $\pi h_{11/2} g_{7/2} \nu h_{11/2}^{-2}$ gives a $\Delta I = 1$ band. In the experiment, only one (with odd spin) signature band is observed for the high-spin part of band N1. This indicates that the configuration assignment of $\pi h_{11/2}^3 g_{7/2}$ for the high-spin part of band N1 is more appropriate. Definitely, to pin down this assignment further experimental information on the electromagnetic transition probabilities is necessary.

Band D2 shows a coupled structure consisting of a series of $\Delta I = 1$ magnetic dipole transitions decaying to bands N1 and N2. The crossover $E2$ transitions cannot be confirmed, leading to large $B(M1)/B(E2)$ ratios. This band exhibits large alignment ($\approx 10\hbar$) and small signature splitting, while the excitation energies lie ≈ 1 MeV above those of the favored branch of band N1. Such a band can be interpreted as a magnetic rotation band built on the $\pi h_{11/2}(g_{7/2}, d_{5/2}) \otimes \nu h_{11/2}^2$ configuration, as several corresponding bands in neighboring ^{132,134}Ba and ^{134,136}Ce [55,65–67] have been reported. In Fig. 11, the alignments and excitation energies of those bands are plotted to show the similarity.

2. Bands N3 and N4

Bands N3 and N4 consist of two odd-spin branches and one even-spin branch. Both odd-spin branches are linked with the even-spin branch by a few $\Delta I = 1$ transitions, showing a similar pattern with bands N1 and N2. Bands N3 and N4 are built on the configuration $\nu h_{11/2}(s_{1/2}, d_{3/2})$, involving another pair of pseudospin partner orbitals $s_{1/2}$ and $d_{3/2}$. However, multiple bands based on the $\nu h_{11/2}(s_{1/2}, d_{3/2})$ configuration can also originate from one neutron occupying different Nilsson orbitals $\nu h_{11/2}[514]9/2$ and $\nu h_{11/2}[523]7/2$ on both sides of the neutron Fermi surface. Coupling the two $\nu h_{11/2}$ Nilsson orbitals with the pseudospin partner orbitals, four configurations are obtained as candidates for bands N3 and N4. PSM calculations have been performed to estimate the excitation energies of the four configurations, in order to make a comparison to experimental data (see Fig. 12). The calculated slope of excitation energies as a function of spin is again higher
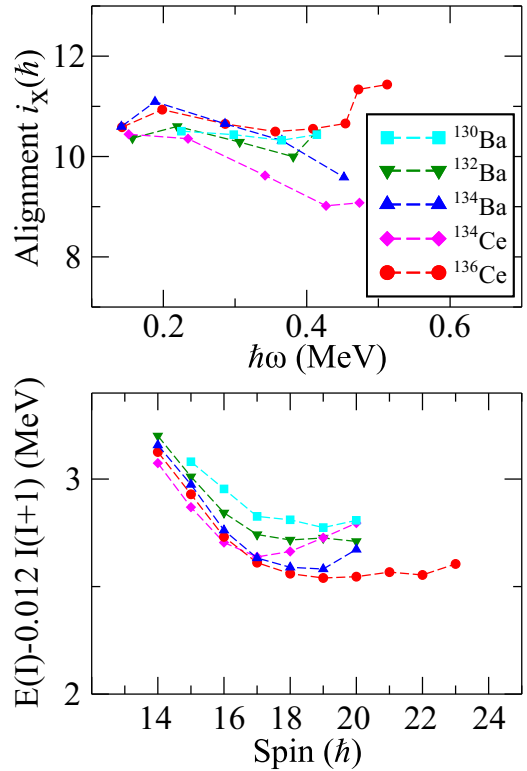

FIG. 11. Alignments (upper panel) and excitation energies refer to a rigid rotor (lower panel) of band D2 and corresponding magnetic rotation bands in ^{132,134}Ba and ^{134,136}Ce. To deduce the alignments, a reference with the Harris parameters $\mathcal{J}_0 = 14 \, \hbar^2\mathrm{MeV}^{-1}$ and $\mathcal{J}_1 = 15 \, \hbar^4\mathrm{MeV}^{-3}$ has been subtracted, and $K = 9$ is assumed.

than the experimental energies. However, according to the calculation, the two configurations involving the $\nu h_{11/2}[514]9/2$ orbital can be ruled out since they have much higher excitation energies than those with $\nu h_{11/2}[523]7/2$. Therefore the bands N3 and N4 can be another pair of pseudospin partner bands built on the $\nu h_{11/2}[523]7/2(s_{1/2}, d_{3/2})$ configuration, with near identical excitation energies for both experimental and calculated results. The slight signature splitting in band
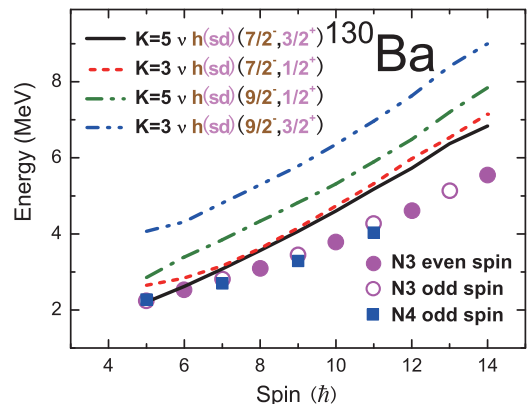

FIG. 12. Calculated excitation energies for configurations achieved by coupling one proton at $\nu h_{11/2}7/2[523]$ or $\nu h_{11/2}9/2[514]$ orbitals and the other at $(s_{1/2}, d_{3/2})$ orbitals, in comparison with the experimental values for bands N3 and N4.
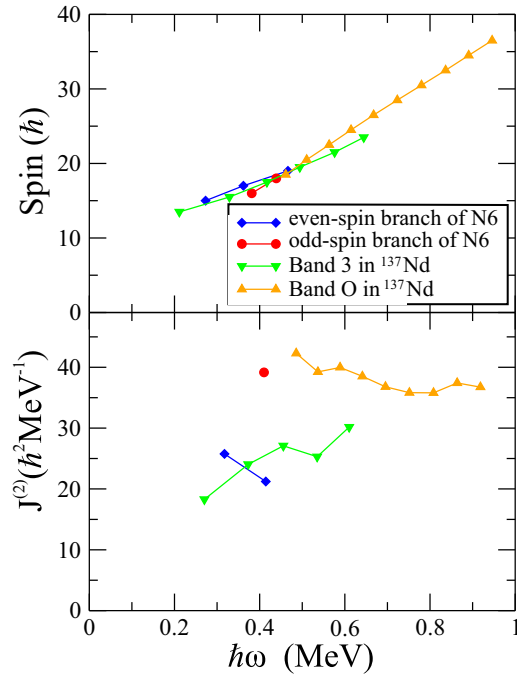
FIG. 13. Spin (upper panel) and the dynamic momenta of inertia (lower panel) versus rotational frequency of the even- and odd-spin branches of band N6, in comparison with those of bands O and 3 in ^{137}Nd.

N3 can be induced by the mixing between band N4 and the odd-spin branch of band N3.

3. Bands N5 and N6

Bands N5 and N6 have been reported and assigned to $\nu h_{11/2}g_{7/2}$ and $\pi h_{11/2}^2 \otimes \nu h_{11/2}g_{7/2}$ configurations, respectively [17,29]. However, anomalous staggering on both the excitation energy and the alignment of band N6 is found, indicating a difference between the even- and odd-spin branches. No linking transitions between the two branches can be confirmed in band N6, whereas intense $\Delta I = 1$ transitions have been observed in band N5. Plotting the spin versus the rotation frequency shows that the slopes for the two branches are different (see Fig. 13). To be more clear, the deduced dynamic moment of inertia on the odd-spin branch is almost double that of the even-spin one. Considering the sharp upbending in the alignments, the interaction between the four-quasiparticle configuration of band N6 and the two-quasiparticle configuration of band N5 would be small. Therefore, no dramatic effect from the interaction between these two configurations

is expected on the deduced moment of inertia. Such behavior reminds us of the recently reported oblate band (band O) in ^{137}Nd, which was interpreted as an antimagnetic rotation band built on the $\pi h_{11/2}^2 \otimes \nu h_{11/2}$ configuration [68]. In the same nucleus, another collective rotational band (band 3) built on either $\pi h_{11/2}^2 \otimes \nu h_{11/2}$ or $\pi h_{11/2}^3$ has been reported [69]. From Fig. 13, it is found that the slopes of spin versus rotation frequency and the moments of inertia of the odd and even branches in ^{130}Ba are similar to those of band O and band 3 in ^{137}Nd, respectively. Therefore, the two branches of band N6 may indicate different motions of the nucleus, namely antimagnetic rotation and collective rotation, based on the same quasi-particle configuration. However, the experimental information is still limited due to the lack of higher spin states. Further experimental and theoretical works are required to make a clear conclusion.

V. SUMMARY

The high-spin structures in ^{130}Ba have been populated via the ^{122}Cd(^{13}C, $5n$) reaction and observed using the GALILEO array. A rich and complete level scheme was established. Two sets of negative-parity doublet bands have been identified. Based on their properties, they are suggested to be pseudospin partner bands built on the $\pi h_{11/2}(g_{7/2}, d_{5/2})$ and $\nu h_{11/2}(s_{1/2}, d_{3/2})$ configurations. Such assignments are further supported by the PSM and PRM calculations.

[1] S. Guo, C. Petrache, D. Mengoni, Y. Qiang, Y. Wang, Y. Wang *et al.*, Phys. Lett. B **807**, 135572 (2020).

[2] S. Frauendorf and J. Meng, Nucl. Phys. A **617**, 131 (1997).

[3] J. N. Ginocchio, Phys. Rev. Lett. **78**, 436 (1997).

[4] B. W. Xiong and Y. Y. Wang, At. Data Nucl. Data Tables **125**, 193 (2019).

[5] Q. Xu, S. J. Zhu, J. H. Hamilton, A. V. Ramayya, J. K. Hwang, B. Qi *et al.*, Phys. Rev. C **78**, 064301 (2008).

[6] C. M. Petrache, G. Lo Bianco, D. Bazzacco, S. Lunardi, R. Menegazzo, M. Nespolo, G. de Angelis, N. Blasi, V. I. Dimitrov, S. Frauendorf, P. Semmes, and J.-y. Zhang, Phys. Rev. C **65**, 054324 (2002).

[7] J. Sun, Y.-J. Ma, T. Komatsubara, K. Furuno, Y.-H. Zhang, W.-P. Zhou *et al.*, Phys. Rev. C **93**, 064301 (2016).

[8] M. A. Cardona, M. E. Debray, G. García Bermúdez, D. Hojman, A. J. Kreiner, H. Somacal *et al.*, Phys. Rev. C **55**, 144 (1997).

[9] W. Hua, X. H. Zhou, Y. H. Zhang, Y. Zheng, M. L. Liu, F. Ma *et al.*, Phys. Rev. C **80**, 034303 (2009).

[10] P. Petkov, P. von Brentano, J. Jolie, and R. V. Jolos, Phys. Rev. C **76**, 044318 (2007).

[11] J. Meng and S. Q. Zhang, J. Phys. G: Nucl. Part. Phys. **37**, 064025 (2010).

[12] S. Sihotra, K. Singh, S. S. Malik, J. Goswamy, R. Palit, Z. Naik, D. Mehta, N. Singh, R. Kumar, R. P. Singh, and S. Muralithar, Phys. Rev. C **79**, 044317 (2009).

[13] H. F. Brinckmann, C. Heiser, K. F. Alexander, W. Neubert, and H. Rotter, Nucl. Phys. A **81**, 233 (1966).

[14] H. Rotter, K. F. Alexander, C. Droste, T. Morek, W. Neubert, and S. Chojnacki, Nucl. Phys. A **133**, 648 (1969).

[15] R. Moore *et al.*, Phys. Lett. B **547**, 200 (2002).

[16] J. Perkovski *et al.*, Acta Phys. Pol. B **43**, 273 (2012).

[17] Y. H. Qiang, C. M. Petrache, S. Guo, P. M. Walker, D. Mengoni, Q. B. Chen *et al.*, Phys. Rev. C **99**, 014307 (2019).

[18] C. Droste, T. Morek, M. Nowicki, E. Sayed, J. Srebrny, and W. Starosta, Acta Phys. Pol. B **5**, 561 (1974).

[19] W. Urban, T. Rzaca, C. Droste, L. Goettig, T. Morek, and J. Srebrny, Z. Phys. A **305**, 335 (1974).

[20] K. Kirch *et al.*, Nucl. Phys. A **587**, 211 (1995).

[21] C. T. Konigshofen, K. Jessen, A. Gade, I. Wiedenhover, H. Meise, and P. von Brentano, Phys. Rev. C **64**, 037302 (2001).

[22] G. Suliman *et al.*, Eur. Phys. J. A **36**, 243 (2008).

[23] X. Sun, D. Bazzacco, W. Gast, A. Gelberg, U. Kaup, A. Dewald, K. O. Zell, and P. von Brentano, Phys. Rev. C **28**, 1167 (1983).

[24] H. El-Samman, V. Barci, A. Gizon, J. Gizon, L. Hildingsson, D. Jerrestam *et al.*, Nucl. Phys. A **427**, 397 (1984).

[25] X. Sun, D. Bazzacco, W. Gast, A. Gelberg, U. Kaup, K. Schiffer, A. Dewald, R. Reinhardt, K. O. Zell, and P. von Brentano, Nucl. Phys. A **436**, 506 (1985).

[26] H. El-Samman, V. Barci, A. Gizon, J. Gizon, R. Kossakowski, Th. Lindblad, and T. Bengtsson, Phys. Lett. B **158**, 459 (1985).

[27] O. Stuch, K. Jessen, R. S. Chakrawarthy, A. Dewald, R. Kühn, R. Krücken *et al.*, Phys. Rev. C **61**, 044325 (2000).

[28] N. Kaur, A. Kumar, G. Mukherjee, A. Singh, S. Kumar, and R. Kaur *et al.*, Eur. Phys. J. A **50**, 5 (2014).

[29] C. M. Petrache, P. M. Walker, S. Guo, Q. B. Chen, S. Frauendorf, Y. X. Liu *et al.*, Phys. Lett. B **795**, 241 (2019).

[30] K. Kumar and J. B. Gupta, Nucl. Phys. A **694**, 199 (2001).

[31] J. B. Gupta, Eur. Phys. J. A **51**, 47 (2015).

[32] E. Hammaren, K. W. Schmid, F. Grummer, A. Faessler, and B. Fleadt, Nucl. Phys. A **454**, 301 (1986).

[33] R. Wyss, A. Granderath, R. Bengtsson, P. von Brentano, A. Dewald, A. Gelberg *et al.*, Nucl. Phys. A **505**, 337 (1989).

[34] A. Granderath, P. F. Mantica, R. Bengtsson, R. Wyss, P. von Brentano, A. Gelberg, and F. Seiffert, Nucl. Phys. A **597**, 427 (1996).

[35] F. R. Xu, P. M. Walker, and R. Wyss, Phys. Rev. C **59**, 731 (1999).

[36] F. Iachello and A. Arima, *The Interacting Boson Model* (Cambridge University Press, Cambridge, 1987).

[37] F. Iachello, Phys. Rev. Lett. **85**, 3580 (2000).

[38] R. F. Casten and N. V. Zamfir, Phys. Rev. Lett. **85**, 3584 (2000).

[39] S. Q. Zhang, B. Qi, S. Y. Wang, and J. Meng, Phys. Rev. C **75**, 044307 (2007).

[40] Q. B. Chen, S. Frauendorf, and C. M. Petrache, Phys. Rev. C **100**, 061301(R) (2019).

[41] A. Gavron, Phys. Rev. C **21**, 230 (1980).

[42] D. Testov, D. Mengoni, A. Goasduff, A. Gadea, R. Isocrate, P. R. John *et al.*, Eur. Phys. J. A **55**, 47 (2019).

[43] O. Skeppstedt, H. A. Roth, L. Lindström *et al.*, Nucl. Instrum. Methods Phys. Res. A **421**, 531 (1999).

[44] J. Ljungvall, M. Palacz, and J. Nyberg, Nucl. Instrum. Methods Phys. Res. A **528**, 741 (2004).

[45] L. Berti, M. Biasotto, S. Fantinel, A. Gozzelino, M. Gulmini, and N. Toniolo, LNL INFN Annual Report, 2014 (unpublished), p. 93.

[46] D. Radford, Nucl. Instrum. Methods Phys. Res. A **361**, 297 (1995).

[47] D. Radford, Nucl. Instrum. Methods Phys. Res. A **361**, 306 (1995).

[48] A. Krämer-Flecken, T. Morek, R. M. Lieder, W. Gast, G. Hebbinghaus, H. M. Jäger, and W. Urban, Nucl. Instrum. Methods Phys. Res. A **275**, 333 (1989).

[49] J. T. Matta, U. Garg, W. Li, S. Frauendorf, A. D. Ayangeakaa, D. Patel *et al.*, Phys. Rev. Lett. **114**, 082501 (2015).

[50] J. T. Matta (private communication).

[51] L. Hildingsson, W. Klamra, T. Lindblad, F. Lidén, Y. Liang, R. Ma, E. S. Paul, N. Xu, D. B. Fossan, and J. Gascon, Z. Phys. A **340**, 29 (1991).

[52] D. Ward, V. P. Janzen, H. R. Andrews, D. C. Radford, G. C. Ball, D. Horn *et al.*, Nucl. Phys. A **529**, 315 (1991).

[53] O. Vogel, R. S. Chakrawarthy, A. Dewald, P. Petkov, K. Jessen, J. Gableske *et al.*, Eur. Phys. J. A **4**, 323 (1999).

[54] P. Möller, A. J. Sierk, T. Ichikawa, and H. Sagawa, At. Data Nucl. Data Tables **109-110**, 1 (2016).

[55] S. Juutinen, S. Törmänen, P. Ahonen, M. Carpenter, C. Fahlander, J. Gascon *et al.*, Phys. Rev. C **52**, 2946 (1995).

[56] E. S. Paul, A. J. Boston, D. T. Joss, P. J. Nolan, J. A. Sampson, A. T. Semple *et al.*, Nucl. Phys. A **619**, 177 (1997).

[57] C. Petrache, D. Bazzacco, S. Lunardi, C. Rossi Alvarez, R. Venturelli, D. Bucurescu *et al.*, Phys. Lett. B **373**, 275 (1996).

[58] B. Qi, S. Q. Zhang, J. Meng, S. Y. Wang, and S. Frauendorf, Phys. Lett. B **675**, 175 (2009).

[59] E. Streck, Q. B. Chen, N. Kaiser, and Ulf-G. Meißner, Phys. Rev. C **98**, 044314 (2018).

[60] Q. B. Chen, B. F. Lv, C. M. Petrache, and J. Meng, Phys. Lett. B **782**, 744 (2018).

[61] Q. B. Chen, N. Kaiser, Ulf-G. Meißner, and J. Meng, Phys. Rev. C **99**, 064326 (2019).

[62] J. Meng, J. Peng, S. Q. Zhang, and S.-G. Zhou, Phys. Rev. C **73**, 037303 (2006).

[63] *Relativistic Density Functional for Nuclear Structure*, edited by J. Meng, International Review of Nuclear Physics (World Scientific, Singapore, 2016), Vol. 10.

[64] P. W. Zhao, Z. P. Li, J. M. Yao, and J. Meng, Phys. Rev. C **82**, 054319 (2010).

[65] Neelam, S. Kumar, K. R. Devi, N. Kumar, S. Saha, S. Biswas *et al.*, Phys. Rev. C **101**, 014312 (2020).

[66] S. Lakshmi, H. C. Jain, P. K. Joshi, A. K. Jain, and S. S. Malik, Phys. Rev. C **69**, 014319 (2004).

[67] S. Lakshmi, H. C. Jain, P. K. Joshi, Amita, P. Agarwal, A. K. Jain, and S. S. Malik, Phys. Rev. C **66**, 041303(R) (2002).

[68] C. M. Petrache, S. Frauendorf, B. F. Lv, A. Astier, E. Dupont, S. Guo *et al.*, Phys. Rev. C **99**, 041301(R) (2019).

[69] C. Petrache, R. Venturelli, D. Vretenar, D. Bazzacco, G. Bonsignori, S. Brant *et al.*, Nucl. Phys. A **617**, 228 (1997).